ЖЭТФ, 2012, том 141, вып. 4, стр. 757–766

Gd^{3+} ELECTRON SPIN RESONANCE SPECTROSCOPY ON $LaO_{1-x}F_xFeAs$ SUPERCONDUCTORS

A. Alfonsov [a,b*], ***F. Murányi*** [c], ***N. Leps*** [a], ***R. Klingeler*** [d], ***A. Kondrat*** [a], ***C. Hess*** [a], ***S. Wurmehl*** [a], ***A. Köhler*** [a], ***G. Behr*** [a], ***V. Kataev*** [a,b], ***B. Büchner*** [a]

[a] *Leibniz Institute for Solid State and Materials Research IFW Dresden, D-01069, Dresden, Germany*

[b] *Zavoisky Physical-Technical Institute, Kazan Scientific Center, Russian Academy of Sciences 420029, Kazan, Russia*

[c] *University of Zürich, CH-8057 Zürich, Switzerland*

[d] *Kirchhoff Institute for Physics, Heidelberg University D-69120, Heidelberg, Germany*

Received July 22, 2011

We report an electron spin resonance (ESR) spectroscopy study on polycrystalline samples of the $LaO_{1-x}F_xFeAs$ ($x = 0$ and 0.1) compound with small levels of Gd doping (2 % and 5 %). The Gd ESR signal is found to be sensitive to the magnetic phase transition from the paramagnetic to the spin density wave (SDW) state occurring in the parent $Gd_{1-y}La_yOFeAs$ compounds at $T_{SDW} \sim 130$ K. Interestingly, the analysis of the low-temperature ESR spectra of the c-axis oriented $Gd_{1-y}La_yOFeAs$ samples gives evidence for the magnetically nonequivalent Gd sites and also for sites having a different local charge environment. The analysis of the temperature dependence of the ESR linewidths gives evidence for a coupling of the localized $4f$ electrons of Gd to the conduction electrons in the FeAs layers. The ESR data reveal that the fluorine substitution, which provides electron doping, suppresses the SDW order and enhances the density of states in the electronic bands stemming from the xz and yz orbital states of Fe to which the $4f$ electrons are most strongly coupled.

1. INTRODUCTION

Superconductivity discovered in Fe pnictides [1] in 2008 has attracted a huge interest to these materials. There are several families of Fe pnictides that all have a common structural element: namely the FeAs layers that are responsible for superconductivity. These layers are sandwiched along the crystallographic c-axis by single-atom layers of Ba, Eu, Ca, etc. (the 122 family, e. g., $BaFe_2As_2$), layers of Li, such as in LiFeAs (the 111 family), or by double atom RO layers in ROFeAs (the 1111 family). Here, R is a rare earth element. In this paper, we focus on a representative of the 1111-type family, $LaO_{1-x}F_xFeAs$. Electron doping in 1111 compounds is achieved by partial substitution of fluorine for oxygen. The parent, undoped compounds are semimetallic and exhibit a magnetic phase transition at a temperature T_{SDW} in the range 120 K–140 K depending on the R element [2–7]. Mössbauer spectroscopy, μSR and neutron diffraction experiments show that the ground state is an antiferromagnetic commensurate spin density wave (SDW) with an ordered Fe magnetic moment $\sim 0.5\mu_B$ [3, 7–9]. The magnetic phase transition is always preceded by a structural transition from the tetragonal to the orthorhombic phase occurring at a temperature T_{ST} that is by 10 K–20 K higher than T_{SDW} [4–7, 10]. The fluorine doping results in a suppression of the SDW order and gives rise to superconductivity with a maximum T_c exceeding 55 K in $SmO_{1-x}F_xFeAs$ [2, 10, 11].

Understanding the nontrivial nature of magnetism in Fe pnictides, which evolves from a long-range static to a slowly fluctuating short-range order type upon charge carrier doping (see, e. g., [11, 12] and the references therein), calls for the use of local probe techniques. In this paper, we explore the possibilities of

*E-mail: a.alfonsov@ifw-dresden.de

electron spin resonance (ESR) spectroscopy to gain insights into the magnetic and electronic properties of $LaO_{1-x}F_xFeAs$. No intrinsic ESR signal associated with the resonance of the Fe moments can be observed in this compound. This is likely because d-electrons stemming from Fe are delocalized in the FeAs layers and experience strong momentum scattering. Owing to a substantial spin–orbit coupling, this could cause a strong spin relaxation and, consequently, very broad ESR linewidths. We therefore introduced a special ESR spin probe in $LaO_{1-x}F_xFeAs$ by doping the samples with a few percent of Gd at a nonmagnetic La site. The Gd^{3+} ion has a half-filled $4f$ shell, which gives rise to the maximum possible spin value $S = 7/2$, whereas the orbital moment L is completely absent. Therefore, the well-localized magnetic moment of Gd has a pure spin nature and is not sensitive to phonon-mediated relaxation processes ($L = 0$). This insensitivity enables observation of the Gd ESR signal even at room and higher temperatures, whereas the characteristics of the ESR signal are selectively sensitive to static and dynamic magnetism in the surrounding of the Gd ion. For these reasons, the ESR of Gd dopants was successfully used in the past for probing local electronic and magnetic properties of superconducting cuprates (see, e. g., [12–18]). Here, we establish the Gd^{3+} ESR as a sensitive probe of local magnetic fields due to the spin density wave in FeAs layers. We determine the value of the corresponding dipolar field at a Gd site, which amounts to ~ 7.8 mT and appears to have an alternating sign. Furthermore, we observe the so-called Korringa relaxation of Gd spins on the conduction electrons, which allows following the changes in the density of states of conduction electrons at the Fermi energy upon the fluorine doping.

2. EXPERIMENTAL SETUPS

The magnetization has been studied by means of a commercial SQUID magnetometer (MPMS-XL5, Quantum Design). In the electrical transport experiments, the samples were investigated by four-probe resistivity ρ measurements using an alternating DC current. The ESR measurements at the frequency $\nu = 9.5$ GHz were carried out with a standard Bruker EMX spectrometer.

3. SAMPLE PREPARATION

The polycrystalline samples of $Gd_{1-y}La_yOFeAs$ ($x = 0$, 0.1 and $y = 0.02$, 0.05 nominal content) were prepared as described in [9,10] using FeAs, Gd, La, La_2O_3, and LaF_3 in a stoichiometric ratio. All materials were homogenized in a mortar. The resulting powders were pressed into pellets in Ar atmosphere, and subsequently annealed in an evacuated quartz tube in a two-step synthesis.

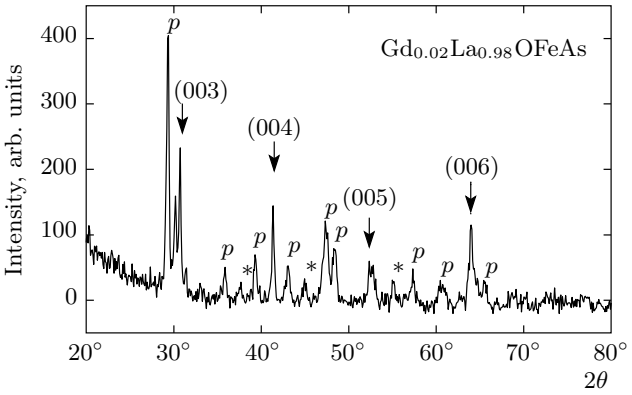

Fig. 1. Powder X-ray diffraction pattern of the c-axis-aligned $Gd_{0.02}La_{0.98}OFeAs$ sample

Due to the complications in crystal growth, the single crystalline samples are not available. To perform ESR experiments where the magnetic field should be applied parallel to the local symmetry axis of the Gd ion (crystallographic c-axis of the compound), we effected the c-axis alignment of the $Gd_{1-y}La_yOFeAs$ ($y = 0.02$ and 0.05) samples. The sample was fine ground to a fine powder, then mixed with epoxy resin, and hardened while rotating in the magnetic field 1.5 T. The X-ray diffraction data of the aligned powder samples were collected at room temperature using a PANalytical X'Pert PRO system (Philips) with Co K_α-radiation (Fig. 1). The presence of highly intense [00l] reflections that dominate the pattern (Fig. 1, arrows) points to a sufficiently high quality of the alignment. Reflections with Miller indices different from [00l] (Fig. 1, asterisks) are also visible in the background, but their intensity is strongly suppressed compared to the pure powder pattern. In the oriented powder pattern, there are additional reflections, marked with the symbol "p". They are attributed to the sample holder (plasticine).

4. SAMPLE CHARACTERIZATION

The temperature dependence of the static magnetic susceptibility χ of 2 % and 5 % Gd-doped LaOFeAs samples is shown in Fig. 2*a*,*b* with squares. It can be fitted with high accuracy using the Curie–Weiss

Table 1. Nominal and actual Gd contents as derived from the magnetization analysis

	Nominal y	Actual y
$La_{1-y}Gd_yOFeAs$	0.020	0.016
$La_{1-y}Gd_yOFeAs$	0.050	0.048
$La_{1-y}Gd_yO_{0.9}F_{0.1}FeAs$	0.050	0.049

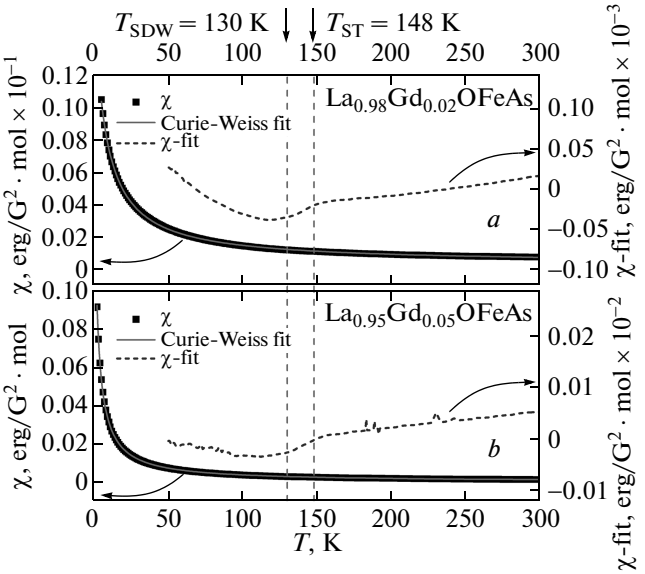

Fig. 2. Magnetic susceptibility data on *a*) a $La_{0.98}Gd_{0.02}OFeAs$ sample and *b*) a $La_{0.95}Gd_{0.05}OFeAs$ sample. The arrows on top point to the structural transition temperature $T_{ST} = 148$ K and to the magnetic phase transition temperature $T_{SDW} = 130$ K

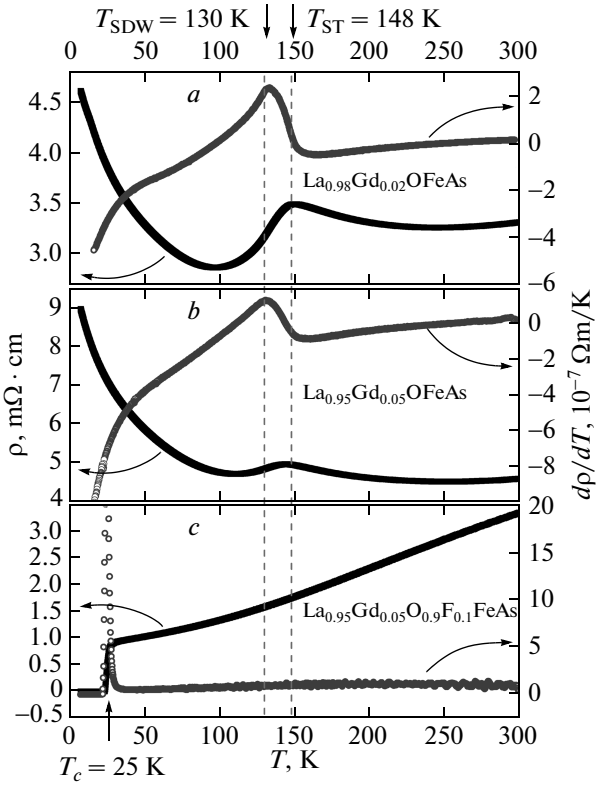

Fig. 3. Electric resistivity data on *a*) a $La_{0.98}Gd_{0.02}OFeAs$ sample, *b*) a $La_{0.95}Gd_{0.05}OFeAs$ sample and *c*) a $La_{0.95}Gd_{0.05}O_{0.9}F_{0.1}FeAs$ sample. The arrows on top point to the structural transition temperature $T_{ST} = 148$ K and to the magnetic phase transition temperature $T_{SDW} = 130$ K

law (solid lines). This fit enables an accurate estimate of the actual Gd content in the sample, which is shown together with the nominal content in Table 1. As can be seen, the real content does not differ significantly from the nominal one in all cases. To label the samples in what follows, we use the nominal content values. By subtracting the Curie–Weiss fit from the measured data, we extract the susceptibility of the FeAs layers $\chi_{Fe} = \chi - \chi_{fit}^{Gd}$ in these samples. The results of the subtraction are shown with dashed lines in Fig. 2*a,b* for both 2 % and 5 % doped LaOFeAs samples. It can be clearly seen that at temperatures in the range 120–150 K, χ_{Fe} experiences characteristic changes: the monotonic quasilinear decrease of the susceptibility turns into a rapid downturn, after which χ_{Fe} begins to increase again. This behavior is quite similar to the known temperature dependence of χ of the parent LaOFeAs samples without Gd doping [7, 19] and is attributed to the respective structural and magnetic phase transitions. But because the Gd magnetic susceptibility overwhelms the susceptibility of the FeAs layers in our samples, it is quite difficult to obtain accurate transition temperatures from the static magnetometery data.

Fortunately, the phase transition temperatures (T_{ST}, T_{SDW}, and T_c) of 2 % and 5 % Gd-doped $LaO_{1-x}F_xFeAs$ samples can be determined more precisely from the electrical resistivity measurements, which are not sensitive to Gd magnetism. In the case of samples without fluorine (Fig. 3*a,b*), the resistivity shows a behavior qualitatively similar to that of the LaOFeAs parent compound [7, 10]. The electrical resistivity exhibits a clear anomaly at $T_{ST} = 148$ K, which is associated with the tetragonal-to-orthorhombic structural phase transition. In addition, the resis-

tivity derivative shows a peak-like anomaly at $T_{SDW} =$ $= 130$ K, related to the magnetic transition. The assignment of the phase transitions is described in Refs. [7, 10]. Compared to the pure LaOFeAs, our Gd-doped samples show somewhat reduced transition temperatures, possibly due to increased disorder in the system. The $Gd_{1-y}La_yO_{1-x}F_xFeAs$ sample with 10 % fluorine doping does not give any evidence of the structural and the SDW transitions, but shows a transition to the superconducting state at $T_c = 25$ K (Fig. 3*c*), similar to what is observed in the Gd-free case [6].

5. ESR MEASUREMENTS AND DISCUSSION

ESR measurements were performed at the X-band frequency ∼9.5 GHz in the temperature range 5–300 K. The typical powder ESR spectra at $T = 130$ K are shown in Fig. 4*a* and Fig. 4*b* for 2 % and 5 % doped samples. To fit the spectra, we used two lines of Dysonian shape, shown as dashed lines in Fig. 4*a,b*. Below, we call them the broad and narrow components. The Dysonian ESR line shape is a result of mixing of absorption and dispersion at the instant of resonance, which occurs if the microwave penetration depth is comparable to or smaller than the sample size. This is typical for the conducting systems like the present samples. The peculiar line shape and the necessity to use two lines for a fit are explained by the powder averaging of the fine structure of the Gd ESR signal. Because Gd^{3+} is a spin-only ion with $S = 7/2$ and $L = 0$, the value of its isotropic g-factor is very close to 2.

The 8-fold degeneracy of the spin levels in the ground state is lifted by the crystal field (CF) only slightly due to the small admixture of the high-energy multiplet with $L > 0$ [20, 21]. In this case, the CF potential acts only as a small perturbation to the Zeeman energy, giving rise to a zero field splitting of the Gd energy levels in the ground-state multiplet of the order of 0.01–0.1 mK (see Fig. 5*a*). According to the ESR selection rules ($\Delta S_z = \pm 1$), the ESR spectrum consists of seven absorption lines: the central transition $+1/2 \leftrightarrow -1/2$ with the highest intensity and six satellites $\pm 3/2 \leftrightarrow \pm 1/2$, $\pm 5/2 \leftrightarrow \pm 3/2$ and $\pm 7/2 \leftrightarrow \pm 5/2$. The resonance field of the main transition ($+1/2 \leftrightarrow -1/2$) is almost independent of the angle between the symmetry axis z and the external magnetic field due to the g-factor isotropy (see Fig. 5*b*). By contrast, the satellites change their positions under rotation of the magnetic field with respect to z from $H \parallel z$ to $H \perp z$. Hence, the powder averaging of the spectra leads to its transformation to the shape shown in Fig. 4*a,b* (see also, e. g., [22]).

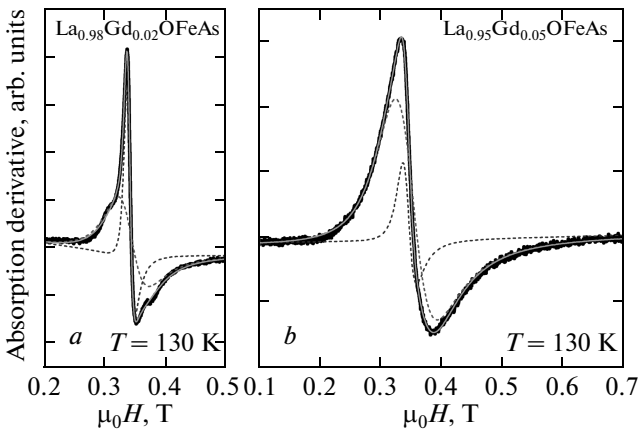

Fig. 4. Experimental ESR spectra (data points) and a two-component fit of the spectra (dashed lines) of *a*) $La_{0.98}Gd_{0.02}OFeAs$ and *b*) $La_{0.95}Gd_{0.05}OFeAs$

Information on the CF splitting and the accurate value of the magnetic field acting on the Gd ion, which actually defines the position of the central line, can be extracted from the two-component fit of the Gd ESR signal. The narrow component models the main transition. Its resonance field is determined by the local field at the Gd site. The broad component mimics the effect of the powder averaging of the satellites. Various contributions to the powder ESR linewidth can exist in metals [22]. Therefore, the width of the broad component measures the crystal field splitting, the local magnetic field, if there are magnetically nonequivalent Gd sites and the Korringa relaxation process (see below).

In Fig. 6*a,b*, the temperature dependences of the resonance field of the narrow component H_{res} and of the width δH of the broad component are shown for the 2 % and 5 % Gd-doped LaOFeAs samples. H_{res} is practically constant down to the magnetic phase transition temperature $T_{SDW} = 130$ K, where it begins to shift to lower fields. The shift amounting to ≈ 7 mT is similar for both samples. At temperatures above T_{SDW} and T_{ST}, the width δH of the broad and narrow components decreases linearly in T as the temperature decreases (Fig. 6*b*). This kind of behavior occurs when localized magnetic moments in a metallic host interact with conduction electrons. This interaction causes the so-called Korringa relaxation process [22, 23]. The relaxation-driven part of the linewidth is given by

$$\delta H \sim [N(\epsilon_F)J]^2 T. \qquad (1)$$

According to Eq. (1), the slope $\delta H/dT$ is proportional to the electronic density of states $N(\epsilon_F)$ at the Fermi

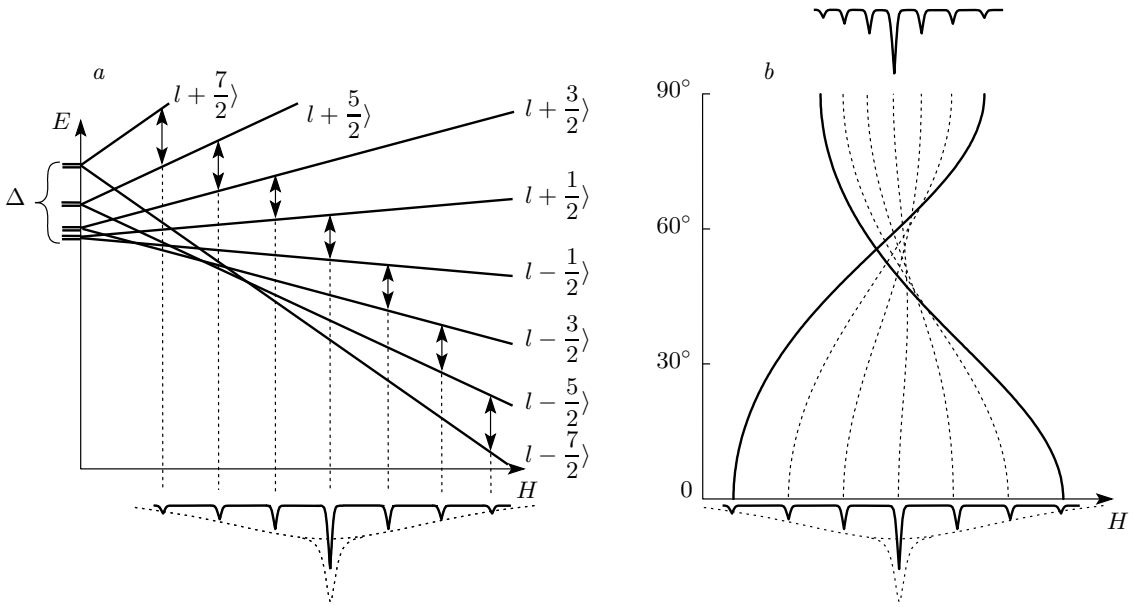

Fig. 5. *a*) Crystal field and Zeeman splitting of the energy levels of the Gd^{3+} ion (top) and the corresponding ESR spectrum arising due to the ESR selection rule $\Delta S_z = \pm 1$ (bottom). *b*) Dependence of the position of the fine structure components of the Gd ESR spectrum on the angle θ between the magnetic field direction and the symmetry axis z; $H \parallel z$ corresponds to $\theta = 0$ and $H \perp z$ corresponds to $\theta = 90^\circ$. Dashed lines in (*a*) and (*b*) are powder-averaged spectra

energy ϵ_F and to the coupling constant J between conduction and localized $4f$ electrons [22, 23]. The Korringa relaxation affects the linewidths of all lines in the fine structure [22]. In our case, in the high-temperature regime $T > T_{SDW}$, both components of the fit of the powder spectrum of the parent, i. e., F-undoped samples compounds exhibit narrowing, which is linear in T (Fig. 6*b*). This suggests that the temperature-dependent part of the linewidth above the SDW transition is determined by the Korringa relaxation of Gd spins due to the interaction with conduction electrons. Here, the Korringa slope is $\delta H/dT \approx 0.045\,\mathrm{mT/K}$. Our finding corroborates the ESR results on $EuFe_2As_2$ single crystals [24], where the spin relaxation of Eu^{2+} ions, which are isoelectronic with Gd^{3+} ions, is also driven by the Korringa mechanism. Notably, the Korringa slope is much bigger in that case, $\delta H/dT \approx 0.8\,\mathrm{mT/K}$, most likely due to a smaller distance between the R layers and the FeAs layers in the 122 family compared to the interlayer distance RO–FeAs in the 1111 family.

As can be seen in Fig. 6*b*, as the temperature decreases below $T_{ST} = 148$ K, the linewidth of the broad component $\delta H(T)$ starts to increase and reveals a jump at $T_{SDW} = 130$ K, which is more pronounced in the case of the 5 % doped sample. This anomaly, albeit much smaller in size, is also visible in the $\delta H(T)$ dependence of the narrow component. Possibly, the initial broadening in this temperature range is due to the change in the fine structure of the Gd^{3+} ESR signal, which is related to the structural transition, whereas the subsequent jump at T_{SDW} can be associated with the magnetic order in the FeAs layers. At even lower temperatures, the linewidths continue to narrow with almost the same $\delta H/dT$ slope as at $T > T_{SDW}$[1)]. This is different from the situation in $EuFe_2As_2$, where the Korringa mechanism ceases to work below T_{SDW}; in Ref. [24], this was ascribed to a spacial confinement of conduction electrons to FeAs layers at $T < T_{SDW}$. Our data suggests that this scenario is not applicable to the LaOFeAs compound. Already above the SDW transition, the conduction electron density at the Gd site in LaOFeAs is much smaller than that at the Eu site in $EuFe_2As_2$, as is evidenced by the differences in the Korringa slopes, but it seems to be unaffected by the SDW transition.

In contrast to the parent compound, the fluorine-doped sample does not reveal any anomalies until reaching the superconducting transition temperature T_c (Fig. 6*c*). The Korringa slope $\delta H/dT$ amounts to $\sim 0.06\,\mathrm{mT/K}$ in this case. This value is appreciably

[1)] A small anomaly at around 60 K visible in the data on the 5 % Gd-doped sample seems to be a sample-specific artefact, which finds no correspondence with other physical properties of the compound.

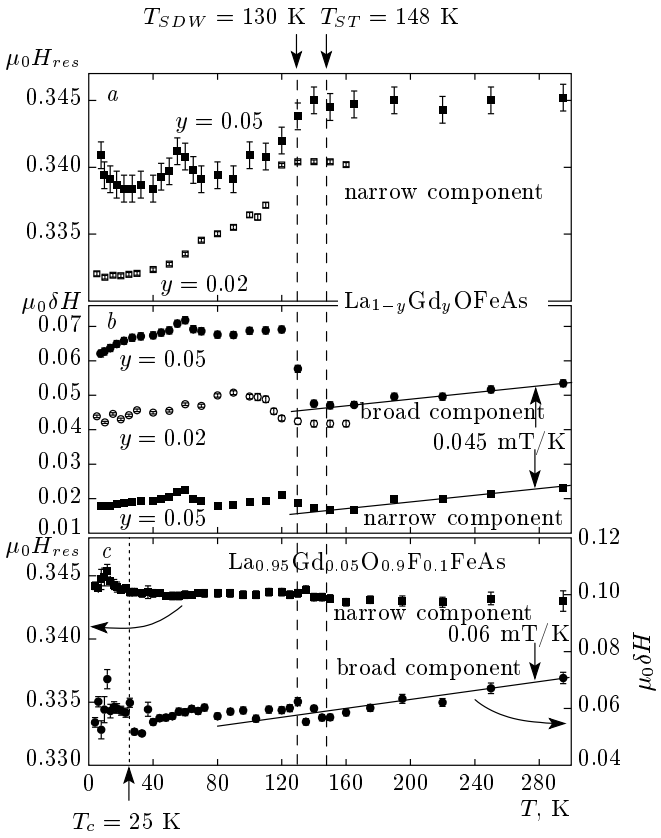

Fig. 6. *a*) Temperature dependence of the resonance field of the narrow component and *b*) the linewidth of both components of Gd-doped LaOFeAs samples; *c*) temperature dependence of the linewidth (right axis) and resonance field (left axis) of the $La_{0.95}Gd_{0.05}O_{0.9}F_{0.1}FeAs$ sample

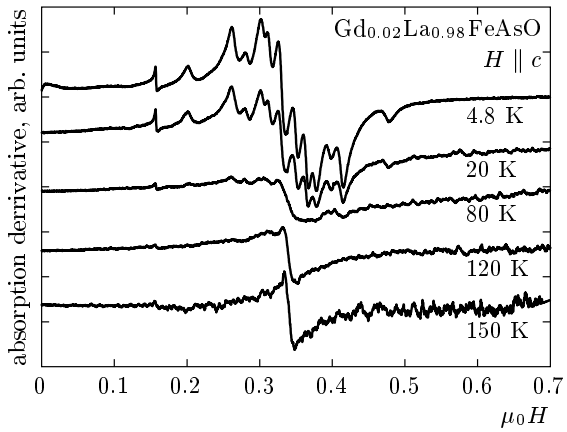

Fig. 7. Temperature dependence of the ESR spectrum of the 2 % Gd-doped *c*-axis-oriented LaOFeAs sample with the magnetic field parallel to the *c*-axis

higher than that in the sample without fluorine. Because $\delta H/dT \propto \sqrt{N(\epsilon_F)}$ according to Eq. (1), the doping of 10 % of fluorine implies an increase in the electronic density of states at the Gd site by about 16 %. At this point, we recall the multi-band character of the electronic states in Fe pnictides. Obviously, the localized $4f$ electrons of Gd interact predominantly with the two "out-of-plane" bands derived from the xz and yz orbital states of Fe, whereas the xy "in-plane" band should be much less effective in the Korringa relaxation. The enhancement of the Korringa relaxation upon the fluorine doping suggests that the doped electrons are not confined exclusively to the FeAs planes and indicates a 3-dimensional character of the electronic density of states.

To resolve the Gd^{3+} fine structure, we have measured ESR on the *c*-axis-oriented 2 % and 5 % Gd-doped LaOFeAs samples. At temperatures above T_{SDW} and T_{ST}, a single Lorentzian line[2)] without a fine structure is observed. The fine structure is not seen most likely because of the Korringa broadening of individual components in the high-temperature regime, and also because of the poor signal-to-noise ratio due to a small susceptibility of Gd ions at high temperatures in this strongly diluted sample. A reduction of the Korringa relaxation together with a concomitant $1/T$ increase of the Gd susceptibility upon cooling enables observation of the Gd^{3+} ESR fine structure below $T \sim 80$ K (Fig. 7). As expected, the resolution of the fine structure depends on the concentration of Gd ions and on the orientation of the magnetic field with respect to the crystallographic directions.

As can be seen in Fig. 8*a*,*b*, the best resolution is achieved for the smallest Gd concentration of 2 % and for the direction of the external field parallel to the orientation axis of the samples (the *c*-axis). In this case, at least 12 absorption lines are visible in the spectrum[3)]. Remarkably, the ESR spectrum of a single Gd^{3+} ion, according to its spin value $S = 7/2$, should comprise at most 7 lines. We note that no additional forbidden transitions ($\Delta S_z = \pm 2, \pm 3 \ldots$) are expected in this

[2)] Because of the fine grinding of the powder and its dilution in the epoxy resin for the purpose of orientation in the magnetic field, the microwaves can thus fully penetrate in the interior of the oriented sample. Therefore, the ESR lineshape changes from a Dysonian to a Lorentzian.

[3)] On the ESR spectra measured at $T = 4$ K, shown in Fig. 8*a*,*b*, we see that in contrast to other lines, the ESR line at the field 1.5 T does not exhibit any changes upon changing the angle θ between the magnetic field and the *c*-axis of the sample. This suggests that this line is not a part of the Gd spectrum and, most probably, is an artefact signal due to a small amount of uncontrollable Fe impurity.

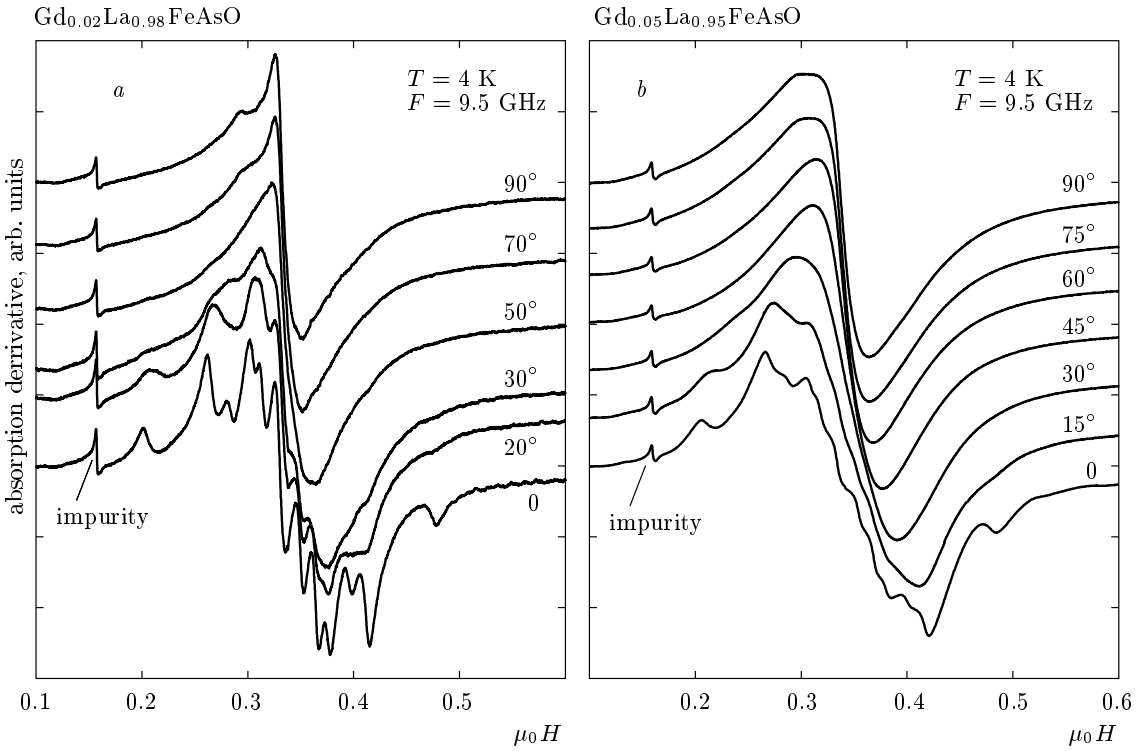

Fig. 8. Angular dependence of the ESR spectra at low temperature of *a*) the 2 % and *b*) 5 % Gd-doped *c*-axis-oriented LaOFeAs sample. θ is the angle between the magnetic field direction and the *c*-axis

case because the external magnetic field is parallel to the symmetry axis [20, 21]. A straightforward explanation for the excess number of the ESR lines is possible assuming the presence of magnetically nonequivalent Gd sites. Indeed, they can arise due to the antiferromagnetic SDW order in the FeAs layer. According to the known alignment of Fe spins in the SDW, which is similar in the entire 1111 family of Fe-based superconductors (see, e. g., [3, 9]), there are two magnetically nonequivalent positions of the R ion, which experience a local internal field of alternating sign induced by the ordered Fe moments. The arrangement of Fe spins in the FeAs layers and of local fields at the R site are sketched in Fig. 9.

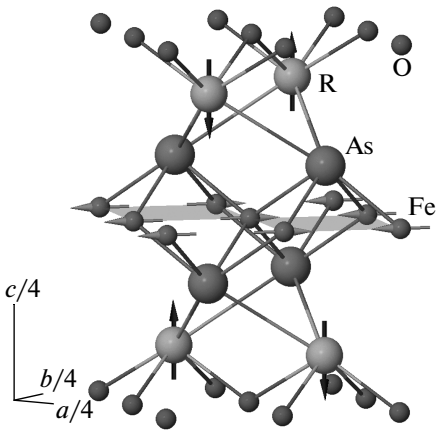

Fig. 9. ROFeAs crystallographic structure with two magnetically nonequivalent R sites (R = La, Gd). Arrows at the R site show the dipolar field produced by the SDW in the FeAs layer. The SDW is schematically shown by the arrows at the Fe sites

To prove this conjecture, we have performed a simulation of the low-temperature Gd^{3+} ESR spectrum assuming two magnetically nonequivalent Gd sites. According to the local crystal field symmetry [25, 26], the energy levels of the Gd^{3+} ion can be described using the effective spin Hamiltonian of the form [20, 21]

$$\mathcal{H}_{eff} = g\mu_B \mathbf{H} \cdot \mathbf{S} + B_2^0 O_2^0 + B_4^0 O_4^0 + B_6^0 O_6^0. \qquad (2)$$

The first term in (2) accounts for the Zeeman interaction. Here, g is a g-factor, μ_B is the Bohr magneton, $\mathbf{H}$ is the sum of the applied magnetic field H_0 and the internal field H_{int}, and $\mathbf{S}$ is the spin. In the next terms in (2), O_n^m are Stevens operators describing the sym-

Table 2. Fitting parameters B_n^m

	B_2^0 (MHz)	B_4^0 (MHz)	B_6^0 (MHz)
CFP	−84.0	−0.185	−0.0055
CFP1	−84.0	−0.185	−0.0055
CFP2	−171.0	−0.40	−0.0045

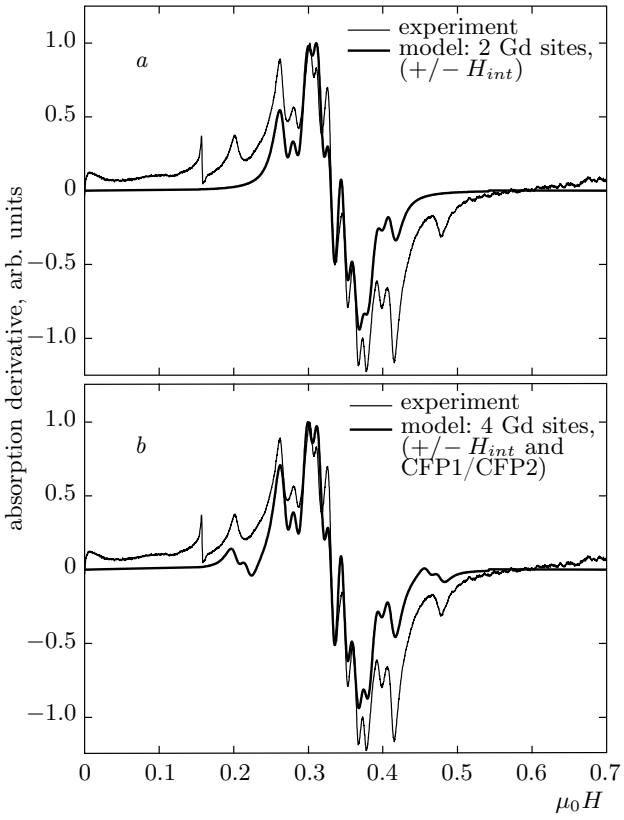

Fig. 10. Simulation of the low-temperature ESR spectrum of the c-axis-oriented 2 % Gd-doped LaOFeAs sample with a) two nonequivalent Gd sites with the alternating internal magnetic field $\pm H_{int}$ and b) four nonequivalent Gd sites described by two sets of crystal field parameters (CFP1 and CFP2) and the alternating internal magnetic field $\pm H_{int}$ at each site

metry of the crystal field and B_n^m are phenomenological crystal field parameters (CFP).

The best modeling of the experimental ESR spectra, taking two magnetically nonequivalent positions into account, is shown in Fig. 10*a*. The set of CFP used for this simulation is presented in Table 2. The g-factor obtained from the fit is equal to 1.99, which is the usual value for the Gd^{3+} ion [20–22]. The internal magnetic field obtained from this simulation is $H_{int} \sim 7.8$ mT. It is interesting to compare this value with the expected strength of the dipolar field H_d at the R site due to the antiferromagnetically ordered Fe moments. With the known positions of the atoms in the unit cell of LaOFeAs and the magnitude of the ordered Fe moment, it is possible to calculate H_d using the formula

$$\mu_0 H_i = \frac{\mu_0}{4\pi}\left(\frac{3(\mathbf{m}\cdot\mathbf{r})}{r^5} i - \frac{m_i}{r^3}\right), \quad i = x, y, z, \qquad (3)$$

where H_i $(i = x, y, z)$ is the component of the magnetic field H_d created by the magnetic dipole moment in the Cartesian coordinate system, $\mathbf{r}$ is the vector connecting the position of the dipole and the point where the magnetic field is calculated, and $\mathbf{m}$ is the vector of the magnetic moment. Under the assumption that Fe moments are point-like dipoles of the strength $0.5\mu_B$ located just at the crystallographic position of Fe, the dipolar calculation according to Eq. (3) yields the value of the internal dipole field 38 mT. This value is much larger than that obtained from the modeling of the ESR spectrum. This is not surprising because in the antiferromagnetically ordered FeAs layers, the spin density is largely delocalized in the form of the SDW, which reduces the dipolar field acting on the Gd ions compared to the point-like dipole approximation. To obtain the agreement with the measured value, the substantially reduced value $0.1\mu_B$ of the Fe magnetic moment must be used in Eq. (3).

The model Gd ESR spectrum shown in Fig. 10*a* reproduces the main features of the experimental spectrum rather well. But it lacks the left and right outermost lines at 0.2 T and 0.48 T, respectively. To account for them, we have to assume the occurrence of an additional Gd site with a distinct crystal field, also subjected to an alternating internal field. This assumption allows reproducing all lines in the experimental spectrum (Fig. 10*b*). The best agreement is achieved with the sets of the crystal field parameters CFP1 and CFP2 listed in Table 2. The spectral weight of the additional crystallographic site with CFP2 is about 30 % of the main site with CFP1. We note that the second site is characterized by a much larger uniaxial second-order and fourth-order CF parameters B_2^0 and B_4^0, compared to the main site (Table 2). Because a unique crystallographic R site is expected in the regular structure, it is feasible that these additional sites are located at (or close to) the surface of the fine powder particles of the oriented samples. Such sites could have a substantial weight in the micron-size particles owing to the enhanced surface-to-volume ratio.

6. SUMMARY

The ESR measurements of lightly Gd-doped samples of the $LaO_{1-x}F_xFeAs$ compound, which is a representative of the 1111 family of Fe pnictide superconductors, establish Gd^{3+} ions as a sensitive ESR probe of magnetic, structural and electronic properties of this compound. In the parent, i. e., not fluorine-doped, samples, the change of the extent of the Gd^{3+} ESR fine structure reflects the occurrence of the structural phase transition. In addition, the antiferromagnetic SDW order manifests itself in the shift and broadening of the powder spectra and in the additional splitting of the fine structure of the ESR spectrum of the c-axis-oriented sample. The analysis of these spectra yields two magnetically nonequivalent R sites at low temperatures due to the SDW order in the FeAs layer. The spin density wave creates a dipolar field alternating in space, of the order of $\sim 7.8\,\text{mT}$ on the Gd ions. Additional features in the spectra could be assigned to the occurrence of Gd sites with distinct crystal field parameters, which are possibly located at the surface of the fine powder particles of the oriented samples. The coupling of the localized $4f$ electrons of Gd to the conduction electrons is manifested by an increase in the linewidths linear in T due to the Korringa relaxation mechanism. The data give evidence that the electronic density of states at the R site in LaOFeAs is significantly reduced compared to the 122-family representative $EuFe_2As_2$. The ESR measurements on the fluorine-doped sample reveal an enhancement of the Koringa slope of the $\delta H(T)$ dependence, implying an increased density of electronic states at the Fermi energy with respect to the parent samples. Taking a multi-band character of the electronic structure of Fe pnictides into account, this finding implies that the electrons doped due to the F substitution contribute to the density of states of the "out-of-plane" bands stemming from the xz and yz orbital states of Fe to which the localized $4f$ electrons are mostly coupled.

We thank S. Müller-Litvanyi, R. Müller, J. Werner, M. Deutschmann, and S. Pichl for the assistance support in sample preparation. We thank U. Stockert and J. E. Hamann-Borrero for the assistance in sample characterization. The work at the IFW Dresden was supported by the Deutsche Forschungsgemeinschaft through Grants No. BE1749/12, the Research Unit FOR538 (Grant No. BU887/4) and the Priority Programme SPP1458 (Grant No. GR3330/2, BE1749/13). Work at the ETH was supported by the Swiss National Science Foundation through the National Center of Competence in Research MaNEP (Materials with Novel Electronic Properties).

REFERENCES

1. Y. Kamihara, T. Watanabe, M. Hirano et al., J. Amer. Chem. Soc. **130**, 3296 (2008).
2. X. H. Chen, T. Wu, G. Wu et al., Nature (London) **453**, 761 (2008).
3. C. de la Cruz, Q. Huang, J. W. Lynn et al., Nature (London) **453**, 899 (2008).
4. J. Zhao, Q. Huang, C. de la Cruz et al., Nature Materials **7**, 953 (2008).
5. M. A. McGuire, A. D. Christianson, A. S. Sefat et al., Phys. Rev. B **78**, 094517 (2008).
6. H. Luetkens, H.-H. Klauss, M. Kraken et al., Nature Materials **8**, 305 (2009).
7. H.-H. Klauss, H. Luetkens, R. Klingeler et al., Phys. Rev. Lett. **101**, 077005 (2008).
8. N. Qureshi, Y. Dress, J. Werner et al., Phys. Rev. B **82**, 184521 (2010).
9. H. Maeter, H. Luetkens, Y. G. Pashkevich et al., Phys. Rev. B **80**, 094524 (2009).
10. A. Kondrat, J. E. Hamann-Borrero, N. Leps, et al., Europ. Phys. J. B **70**, 461 (2009).
11. A. J. Drew, C. Niedermayer, P. J. Baker et al., Nature Materials **8**, 310 (2009).
12. A. Alfonsov, F. Murányi, V. Kataev et al., Phys. Rev. B **83**, 094526 (2011).
13. V. E. Kataev, Y. S. Greznev, E. F. Kukovitskii et al., JETP Lett. **56**, 385 (1992).
14. V. Kataev, Y. S. Greznev, G. Teitel'baum et al., Phys. Rev. B **48**, 13042 (1993).
15. V. Kataev, B. Rameev, B. Büchner et al., Phys. Rev. B **55**, R3394 (1997).
16. V. Kataev, B. Rameev, A. Validov et al., Phys. Rev. B **58**, R11876 (1998).
17. A. Jànossy, L.-C. Brunel, J. R. Cooper et al., Phys. Rev. B **54**, 10186 (1996).
18. A. Jànossy, F. Simon, T. Fehér et al., Phys. Rev. B **59**, 1176 (1999).
19. R. Klingeler, N. Leps, I. Hellmann et al., Phys. Rev. B **81**, 024506 (2010).

20. S. A. Altshuler and B. M. Kozyrev, *Electron Paramagnetic Resonance in Compounds of Transition Elements*, 2nd ed. Wiley, New York (1974).

21. A. Abragam and B. Bleaney, *Electron Paramagnetic Resonance of Transition Ions* (1970).

22. S. E. Barnes, Adv. Phys. **30**, 801 (1981).

23. J. Korringa, Physica **16**, 601 (1950).

24. E. Dengler, J. Deisenhofer, H.-A. Krug von Nidda et al., Phys. Rev. B **81**, 024406 (2010).

25. T. Nomura, S. W. Kim, Y. Kamihara et al., Supercond. Sci. Technol. **21**, 125028 (2008).

26. C. Hess, A. Kondrat, A. Narduzzo et al., Europ. Lett. **87**, 17005 (2009).